Visual Contrast Detection Cannot Be Predicted From Surrogate Measures of Retinal Ganglion Cell Number and Sampling Density in Healthy Young Adults

Jonathan Denniss,[1–3] Andrew Turpin,[2] and Allison M. McKendrick[1]

[1]Department of Optometry and Vision Sciences, University of Melbourne, Melbourne, Australia
[2]Department of Computing and Information Systems, University of Melbourne, Melbourne, Australia
[3]Visual Neuroscience Group, School of Psychology, University of Nottingham, Nottingham, United Kingdom

Correspondence: Jonathan Denniss, Visual Neuroscience Group, School of Psychology, University of Nottingham, Nottingham, UK; jonathan.denniss@nottingham.ac.uk.

Submitted: July 28, 2014
Accepted: October 27, 2014

Citation: Denniss J, Turpin A, McKendrick AM. Visual contrast detection cannot be predicted from surrogate measures of retinal ganglion cell number and sampling density in healthy young adults. *Invest Ophthalmol Vis Sci*. 2014;55:7804–7813. DOI:10.1167/iovs.14-15339

Purpose. To establish whether a clinically exploitable relationship exists between surrogate measures of retinal ganglion cell number and functional sampling density and visual contrast sensitivity in healthy young eyes.

Methods. Psychometric functions for contrast detection were measured at 9° eccentricity in superior and inferior visual field from 20 healthy adults (age 23–43, median 26 years). Functions were compared with corresponding localized regions of retinal nerve fiber layer (RNFL) thickness measured by optical coherence tomography, a surrogate of retinal ganglion cell number, and to grating resolution acuity, a psychophysical surrogate of retinal ganglion cell sampling density. Correlations between psychometric function parameters and retinal ganglion cell surrogates were measured by Spearman's rank correlation.

Results. All measures exhibited a 2- to 4-fold variation in our sample. Despite this, correlations between measures were weak. Correlations between psychometric function parameters (threshold, spread) and RNFL thickness ranged in magnitude from 0.05 to 0.19 ($P = 0.43$–0.85). Grating resolution was sampling limited for 16 of 20 participants in superior visual field, and for 12 of 20 participants in inferior visual field. Correlations between psychometric function parameters and grating resolution acuities ranged in magnitude from 0.05 to 0.36 ($P = 0.12$–0.85) when all data were considered, and from 0.06 to 0.36 ($P = 0.26$–0.87) when only sampling-limited data were considered.

Conclusions. Despite considerable variation in both psychometric functions for contrast detection and surrogate measures of retinal ganglion cell number and sampling density among healthy eyes, relationships between these measures are weak. These relationships are unlikely to be exploitable for improving clinical tests in healthy populations.

Keywords: contrast sensitivity, grating resolution acuity, psychometric functions, retinal ganglion cells, optical coherence tomography

Retinal ganglion cells play a key role in the detection and processing of visual contrast (for example, Refs. 1–4). In glaucoma, the loss of retinal ganglion cells leads to a reduction in contrast sensitivity, clinically measured by perimetry, and also to changes in contrast processing mechanisms, such as contrast gain control and adaptation.[5–10] Further, psychometric functions for detection of perimetric luminance increment stimuli flatten as glaucoma progresses and more retinal ganglion cells are lost.[11,12] Many studies of glaucoma clinical data indicate that a relationship exists between structural imaging measures that aim to infer the number of remaining retinal ganglion cells and perimetric estimates of contrast sensitivity across the visual field (for recent reviews see Harwerth et al.[13] and Malik et al.[14]).

Relating structural and functional measurements is useful clinically for predicting visual function from ocular structure, as long as the association between chosen measures is sufficiently strong. The precision of clinical perimetry is limited by the small number of trials available to estimate threshold, but we have shown that by incorporating prior information from structural measures it may be possible to improve precision of threshold estimates with similar test duration, as long as structural measures can predict the underlying "true" threshold to within approximately ±9 dB.[15] Knowledge of a subject's psychometric function slope is also useful, allowing prediction of the precision of estimates and therefore the use of individual, rather than population-based, limits for the detection of change.[16] Current methods for empirical estimation of psychometric function slope are too time consuming for use in clinical applications such as perimetry,[17] and predicting psychometric function slope from structural measures has not previously been attempted.

Histology has shown that there is at least a 2-fold variation in retinal ganglion cell numbers among healthy adult eyes.[18] The axons of retinal ganglion cells form bundles that course through the retinal nerve fiber layer (RNFL) before exiting the eye via the optic nerve. Although the RNFL also contains significant other tissue, such as glial cells, its thickness, estimated easily by optical coherence tomography (OCT),

TABLE. Details of Each Participant's Age and Refractive Error at Each Tested Eccentricity

Participant	Age, y	Central Refractive Error	Refractive Error 9° Below Central Axis	Refractive Error 9° Above Central Axis
A	42	+0.75DS	Plano/−0.50 × 180	Plano/−0.50 × 180
B	26	−3.75/−0.75 × 40	−4.50/−0.50 × 180	−4.50DS
C	31	−3.00/−1.25 × 40	−3.00/−1.50 × 40	−3.00/−1.50 × 40
D	23	−3.50 DS	−3.50/−0.50 × 160	−3.50DS
E	27	−1.50/−0.50 × 180	−2.25/−0.50 × 180	−2.25/−0.50 × 180
F	26	+0.25DS	Plano	Plano
G	27	+1.25/−0.25 × 180	+0.50/−1.00 × 180	Plano/−0.75 × 180
H	25	+0.50/−0.50 × 180	+0.50/−0.50 × 180	+0.50/−0.50 × 180
I	30	−0.50/−0.25 × 20	−0.50/−0.50 × 180	−0.50/−0.50 × 180
J	28	−1.75DS	−1.50DS	−1.50/−0.50 × 105
K	25	+0.50DS	+0.50	+0.25
L	26	+0.25DS	−0.50DS	Plano/−0.50 × 180
M	28	Plano	−0.75DS	−0.25DS
N	26	−2.25DS	−3.50DS	−3.25
O	23	Plano/−0.75 × 85	−0.50DS	Plano/−0.50 × 120
P	25	−3.00/−1.50 × 10	−3.25/−1.50 × 180	−3.25/−1.50 × 180
Q	26	Plano	Plano	Plano
R	26	+0.50/−0.75 × 90	−0.50/−0.50 × 180	−0.25DS
S	43	−0.50DS	−1.00DS	−0.25/−0.50 × 90
T	32	Plano/−1.00 × 90	−1.00/−0.50 × 90	−0.50/−1.00 × 90

Participants identified as in Figures 2 and 4. Refractive error is given in the form sphere (DS)/cylinder (DC) × axis (degrees).

commonly serves as a surrogate for the total number of retinal ganglion cells in vivo.

In this study, we were interested in whether the variation in retinal structure between healthy individuals bore any consequences for visual function that may be exploitable for improving clinical tests. We measured a regional structural surrogate of retinal ganglion cell number (RNFL from OCT) and a functional surrogate of retinal ganglion cell density (grating resolution acuity) and compared them with psychometric functions for contrast detection measured in corresponding spatial locations. We tested the specific hypotheses that thicker RNFL and greater retinal ganglion cell sampling density would correlate with increased contrast sensitivity and steeper psychometric functions for contrast detection. These hypotheses were tested in a group of young, healthy adults under laboratory, rather than clinical, conditions in an attempt to accurately measure the effects of healthy population variation rather than those of aging or disease.

METHODS

This study was approved by the Human Research Ethics Committee of the University of Melbourne and all participants gave written informed consent to take part in accordance with the tenets of the Declaration of Helsinki. Participants (n = 20, 13 female) were staff and students of the University of Melbourne and had no current or previous eye disease. Participants were aged 23 to 43 years (median 26 years) and had Snellen visual acuity of 6/6 or better in the randomly selected study eye with appropriate refractive correction as necessary that was within the range −5.00 to +5.00 diopters (D) in all meridians and less than 1.50 diopter cylinder (DC) (mean spherical equivalent central refractive error −1.00 D, full details of participant age and refractive error are given in the Table). To optimize the psychophysical measurements taken at 9° above or below fixation, each participant was refractively corrected with large-aperture trial lenses at these eccentricities according to off-axis retinoscopy performed by an experienced optometrist.

All psychophysical stimuli were generated in custom software (MATLAB R2010a; The Mathworks, Natick, MA, USA) and displayed via a visual stimulus generator (ViSaGe; Cambridge Research Systems, Kent, UK) on a gamma-corrected (OptiCal; Cambridge Research Systems) cathode ray tube monitor (LG Flatron 795FT; LG Electronics, Seoul, South Korea) with resolution 1024 × 768 pixels, 31 × 24-cm screen width, refresh rate 100 Hz and mean luminance 50 cd/m^2 in an otherwise dark room. Participants completed all tasks for stimuli presented 9° above and below fixation in separate experimental runs. Fixation was monitored visually via a mirror. All tasks were completed over two to three sessions, each of up to 2 hours' duration and incorporating regular breaks between experimental runs to minimize fatigue.

Measurement of Psychometric Functions for Contrast Detection

Stimuli for the contrast-detection task were randomly generated luminance noise images, band-pass filtered for spatial frequency with a square-wave filter of 1 octave width centered on 2.5 cycles per degree and viewed monocularly from 110 cm (Fig. 1, top left). Stimuli had the same mean luminance as the background and were spatially Gaussian-windowed (SD 0.75°) and static. One hundred such stimuli were pregenerated and one was randomly selected for presentation on each trial. Band-pass luminance noise images were used, as these stimuli contain a wide range of orientation cues, thus eliciting a response from a broad range of retinal ganglion cells, and to operate at spatial frequencies close to the peak of the contrast sensitivity function.[19] Michelson contrast of the stimuli was defined by the formula

$$C = \frac{L_{max} - L_{min}}{L_{max} + L_{min}}, \quad (1)$$

where L represents luminance. Stimuli were presented using a two-interval forced-choice method. On each trial, the stimulus appeared randomly in one of two 200-ms intervals separated by a 500-ms interstimulus interval, and participants were

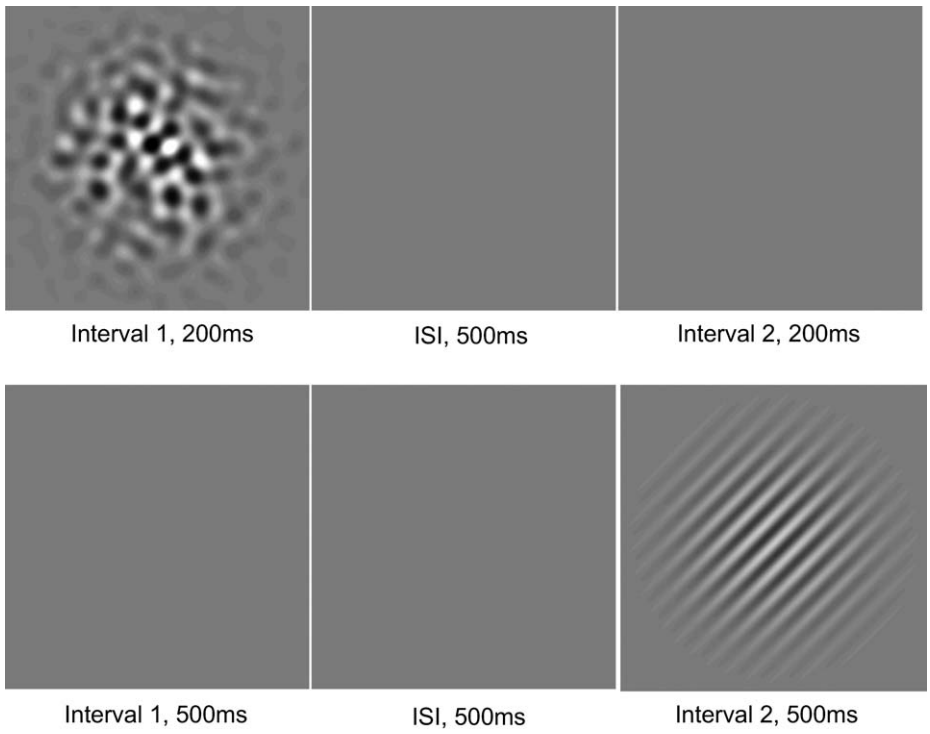

Figure 1. Schematic representation of psychophysical tasks. *Top row*: The stimulus for the contrast-detection experiment was spatial frequency band-pass luminance noise within a Gaussian spatial window (*left*) that varied in contrast, presented randomly in one of two temporal intervals. *Bottom row*: For the grating detection task, the stimulus was a Gabor patch (*right*) that varied in spatial frequency and was presented randomly in one of two temporal intervals. The Gabor patch was oriented randomly at either 45° or 135°. For both tasks, participants reported the interval in which the stimulus appeared. The stimulus for the grating resolution task was the same as for the grating detection task, but presented in a single interval such that the participants' task was to report the orientation of the Gabor.

required to indicate in which interval they saw the stimulus by button press (CB6 response box; Cambridge Research Systems). Psychometric functions were collected using a method of constant stimuli with 10 contrast steps. Experimental runs presented each contrast 10 times in a random order (100 trials per run), and psychometric functions were built up over a minimum of five runs such that each contrast was presented at least 50 times. Before data collection, all participants undertook practice runs.

Psychometric functions were fit in the open-source statistical environment, R (version 2.15.0; R Foundation for Statistical Computing, Vienna, Austria)[20] with the function

$$\psi(x, \mu) = 0.5 + (0.5 - fn) \times [1 - G(x, \mu, s)], \qquad (2)$$

where x represents contrast in %, fn represents the lapse rate defining the upper asymptote, and G represents the fitted cumulative Gaussian function with mean μ and spread (SD) s. Threshold was defined as the 79.4% correct point of the fitted function to facilitate comparison with the grating acuity measures (see later). Fitting was carried out using the glm.WH() function in the *R* package psyphy[21] that follows the procedures recommended by Wichmann and Hill.[22] Fitted psychometric functions' goodness-of-fit was assessed by comparison of model deviance to the deviance distribution of 10,000 Monte Carlo datasets simulated from the fitted function.[22] This method derives empirical probabilities that a dataset of this size generated by the fitted function would have deviance as large or larger than that observed. Higher probabilities therefore indicate better fit. Participants whose psychometric functions had goodness-of-fit P less than 0.05 undertook further trials in an additional session until the fit improved to P greater than 0.05.

Functional Surrogate of Retinal Ganglion Cell Density

Previous studies have demonstrated that spatial aliasing of high spatial frequency grating stimuli occurs in noncentral vision, such that observers can detect the presence of gratings within a certain range of spatial frequencies, but not reliably report their orientation.[23] It is commonly held that under such conditions, the limitation to resolving a grating's orientation is the sampling frequency of the coarsest array of detecting neurons in the retina, which, beyond approximately 8 to 10° eccentricity, is the retinal ganglion cells (see Thibos[24] or Anderson[25] for review). We therefore measured grating detection and resolution acuities at the same locations as for contrast detection, to obtain a functional surrogate estimate of retinal ganglion cell sampling density.

Stimuli for the grating detection and resolution tasks were Gabor patches with 0.75° SD of the Gaussian spatial envelope, presented for 500 ms in total, including 100 ms onset and offset periods in which Michelson contrast was linearly ramped to/from a peak of 95% (Fig. 1, bottom right). Stimuli were viewed monocularly from 220 cm, using an external fixation target. For both tasks, acuities were determined by four interleaved three up, one down staircases, each terminating after seven reversals. Gabor spatial frequency was adjusted by 30% after the first reversal, 20% after the second reversal, and 10% after subsequent reversals. The mean and 95% confidence interval of the final four reversals of each staircase was taken as the acuity (converging on 79.4% correct).

For the grating detection task, stimuli were presented using a two-interval forced-choice method with a 500-ms interstimulus interval as for the contrast-detection task. For the grating resolution task, stimuli were presented using a single interval,

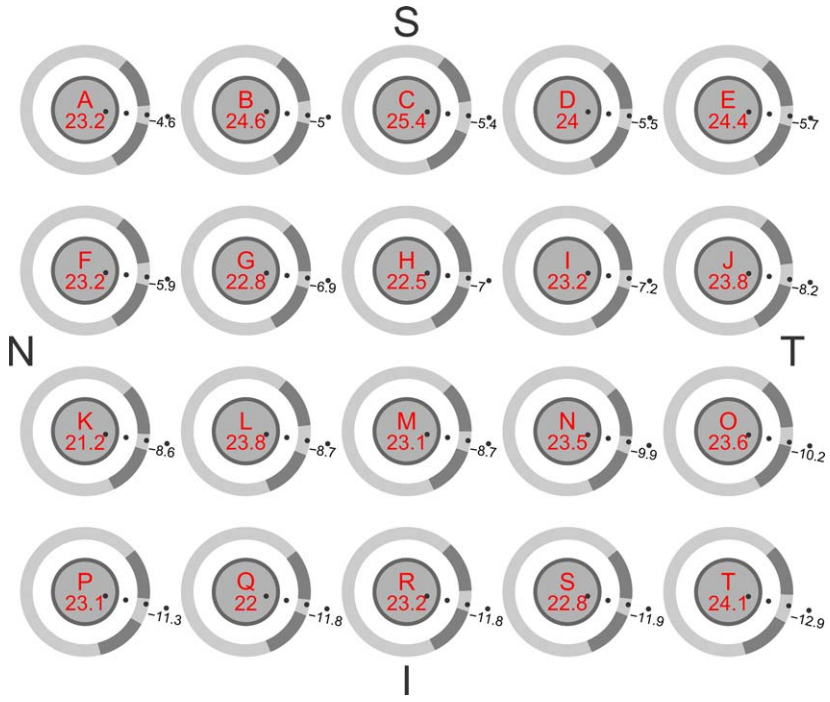

Figure 2. Schematic representation of the RNFL sectors analyzed for each participant: 45° RNFL sectors are shown as *darker-shaded regions* on the outer (scan) circles for each schematic optic nerve head. Participant identifiers and axial lengths are shown in *red*. The *dotted lines* and *black numbers* indicate the angle of the fovea-optic nerve head axis (degrees). S, superior; T, temporal; I, inferior; N, nasal. Participants are arranged throughout this article in order of fovea-optic nerve head angle.

two alternative forced-choice method, whereby participants indicated the orientation of the Gabor by button press. In both tasks, stimulus orientation was randomly chosen on each trial to be either 45° or 135°, and two staircases started from 8.5 cycles per degree and two from 16.0 cycles per degree. For both tasks, all participants took practice runs before data collection. A schematic of the psychophysical tasks is shown in Figure 1.

Structural Surrogate of Retinal Ganglion Cell Number

Retinal nerve fiber layer thickness was measured by OCT (Spectralis; Heidelberg Engineering GmbH, Heidelberg, Germany) around a 12° diameter scan circle manually centered on the optic nerve head. Scans were captured ensuring that the fundus image was evenly illuminated and well-focused, and that the OCT image quality was >20 dB. Any poor-quality scans were recaptured. Images also were manually checked for layer segmentation errors, although none were found. To restrict the region of measured RNFL to that corresponding to the regions of retina tested psychophysically, we used our previously described model that relates regions of the visual field to the optic nerve head, customized to the anatomy of individual eyes.[26,27] In light of recent evidence concerning the position of the temporal raphe in human eyes[28] (Tanabe F, et al. *IOVS* 2014;55: ARVO E-Abstract 957), we made one change to the model as previously published; the raphe temporal to the fovea was set such that the angle between it and the fovea–optic nerve head axis was 170° rather than 180°. The model-predicted 45° RNFL sectors centered on the visual field locations ±9° above fixation, based on individual measurements of axial length (AL-100 biometer; Tomey, Nagoya, Japan) and optic nerve head position (estimated from the OCT images[29]). Previous work has shown that these sectors are more than large enough to compensate for likely measurement error in anatomical measurements.[29] Mean RNFL thickness within the model-predicted 45° sectors was compared to psychophysical measurements (see later).

Statistical Analysis

Correlations between variables were assessed using Spearman's rank correlation, which does not assume linearity of relationships, and is relatively unaffected by outliers because they are maximally assigned the value of their rank only. The 95% confidence intervals for correlation coefficients (ρ) were calculated via the Fisher transformation as

$$\tanh\left(\operatorname{atanh}(\rho) \pm \frac{1.96}{\sqrt{(n-3)}}\right). \quad (3)$$

Correlations for all measures were calculated separately for superior and inferior measurements. For grating resolution acuity, correlations also were calculated both considering all data or only data that were from sampling-limited regions. A region was defined as sampling limited if its grating detection acuity was greater than its grating resolution acuity, with P less than 0.05 by two-tailed Welch's t-test. All analyses were carried out in R (version 2.15.0; R Foundation for Statistical Computing).[20]

Results

Figure 2 shows the two 45° RNFL sectors used for each participant. The two retinal locations tested (9° above and below fixation) vary by only a small amount in their mapping to the optic nerve head across the range of anatomy among the study participants.[27]

Participants had no difficulty with the contrast-detection task, and well-fitting psychometric functions (goodness-of-fit P

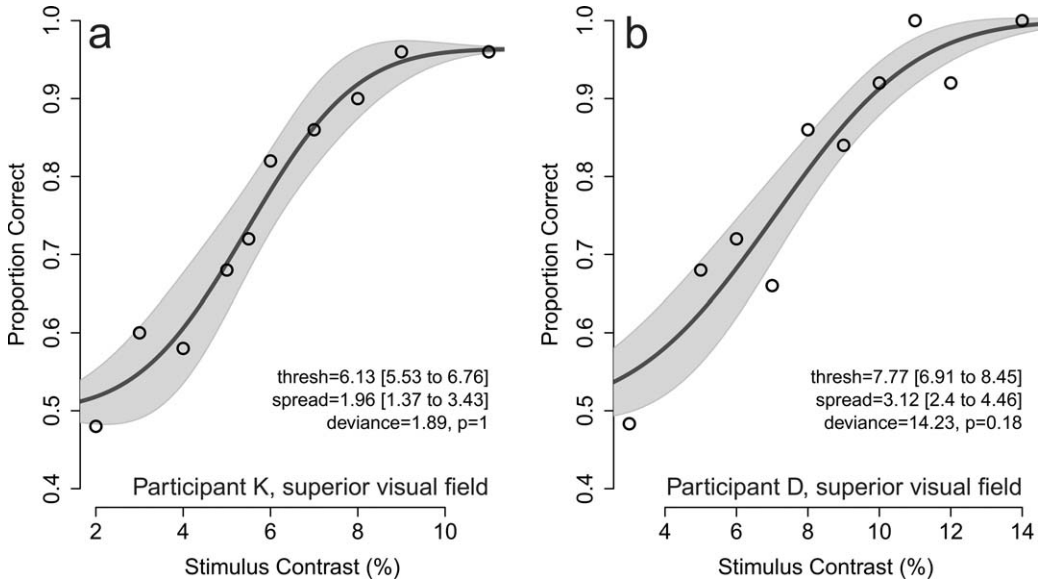

Figure 3. (**a**) Best ($P = 1.0$) and (**b**) worst ($P = 0.18$) fitting individual psychometric functions collected in the contrast-detection experiment. The *dark gray lines* show the best fits of equation 2 to the data, with 95% confidence intervals shown as the *light gray regions*.

$= 0.18$ to $P = 1.0$) were obtained for all superior and inferior contrast-detection measurements. Figure 3 shows the best- and worst-fitting psychometric functions obtained. Contrast-detection thresholds varied from 3.85% to 10.83% for stimuli in the superior visual field, and from 4.04% to 8.72% for stimuli in the inferior visual field. Psychometric function spread (defined as SD of the fitted cumulative Gaussian function) varied from 1.11% to 3.50% for stimuli in the superior visual field, and from 0.92% to 4.00% for stimuli in the inferior visual field. There was a slight association between contrast-detection thresholds and psychometric function spread in the superior visual field, but no association in the inferior visual field (Fig. 4).

Figure 5 shows each participant's detection and resolution acuities for gratings in the superior and inferior visual field. Grating resolution was sampling limited (as defined in the Statistical Analysis section) in the superior visual field for 16 of 20 participants, and in the inferior visual field for 12 of 20 participants. The magnitude of differences between grating detection and resolution acuities, previously referred to as the aliasing zone,[24] varied among participants (Fig. 5).

An approximately 2- to 4-fold variation was found among participants in RNFL thickness, contrast-detection thresholds, and psychometric function spreads, and grating resolution acuities for both superior and inferior retina (Figs. 5, 6). Despite this, no meaningful correlation was found between RNFL thickness (Fig. 6) or grating resolution acuities (Fig. 7) and thresholds or spread of psychometric functions for contrast detection. Correlations between grating resolution and contrast-detection parameters did not improve when only sampling-limited locations were considered (Fig. 7). Figure 8 shows the relationship between RNFL thickness and grating resolution acuities. Again, only very weak correlations were found, and these remained weak when only sampling-limited locations were considered.

Discussion

This study compared visual contrast detection with surrogate measures of retinal ganglion cell number (RNFL thickness by

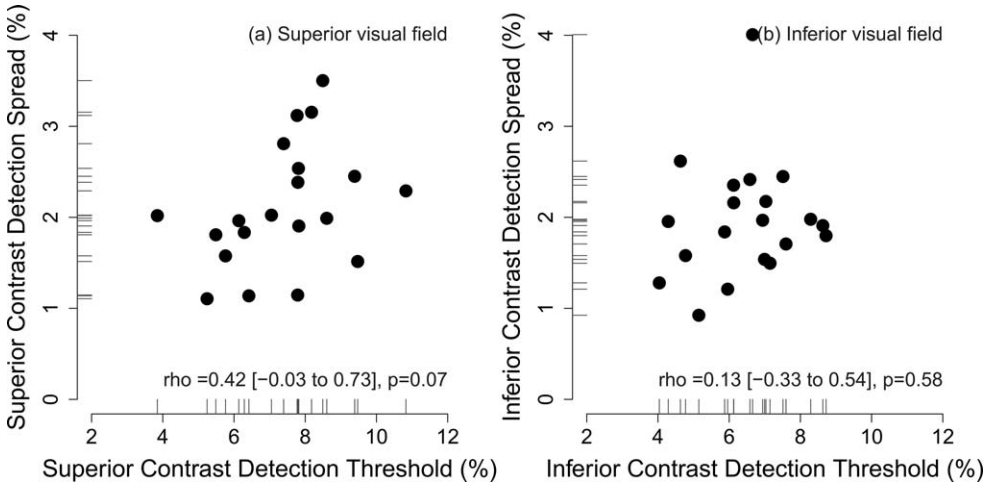

Figure 4. Contrast-detection threshold versus psychometric function spread for (**a**) superior visual field and (**b**) inferior visual field. Spearman's correlations with 95% confidence intervals are given in each panel. *Gray lines* on the axes indicate distributions of the plotted values.

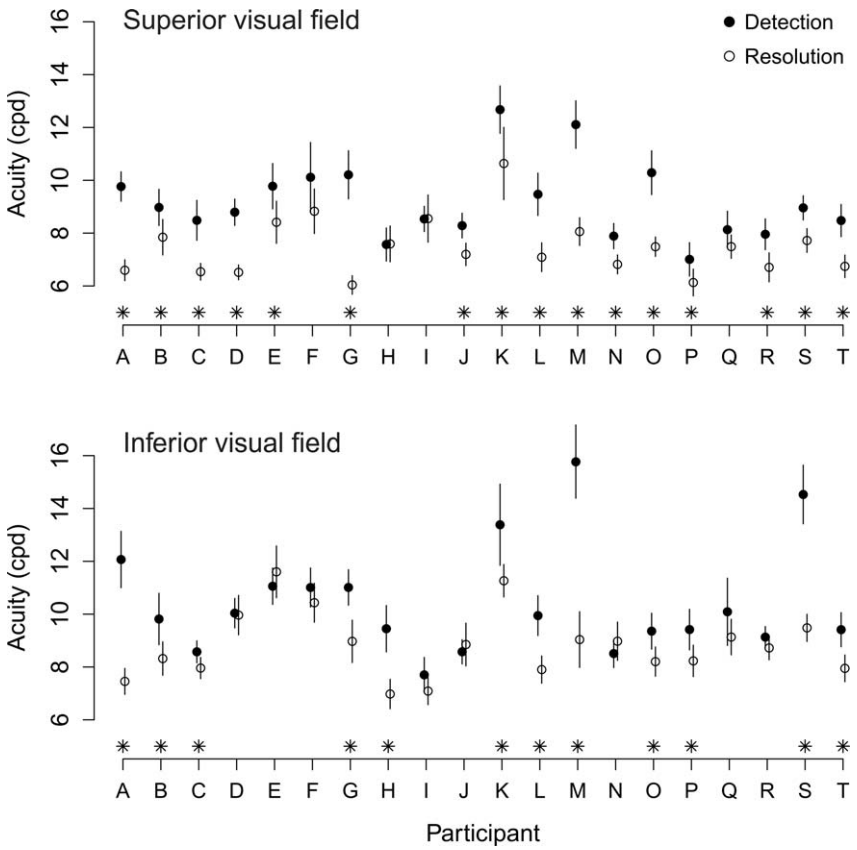

FIGURE 5. Detection and resolution acuities for grating stimuli in superior visual field (*top*) and inferior visual field (*bottom*). Acuities (cycles per degree ±95% confidence intervals) are shown as *filled circles* for detection and *unfilled circles* for resolution. Measurements defined as sampling limited (see text) are marked with an *asterisk* on the *horizontal axis*.

OCT) and sampling density (grating resolution acuity) in a group of healthy young adults. To our knowledge, this is the first report to compare the spread of psychometric functions for contrast detection with surrogates of retinal ganglion cell number. We hypothesized that greater numbers of retinal ganglion cells may have the functional consequence of steeper psychometric functions (smaller spread parameter) due to greater signal in response to a stimulus. The data suggest that any associations between contrast detection and clinically measurable estimates of retinal ganglion cell number or sampling density are very weak in this population. Rank correlations between RNFL thickness and contrast-detection threshold and psychometric function slope ranged in magnitude from 0.05 to 0.19 (Fig. 6). Rank correlations between grating resolution acuity and contrast-detection threshold and psychometric function slope ranged in magnitude from 0.06 to 0.36 when only sampling-limited data were included, and from 0.05 to 0.36 when all data were considered (Fig. 7). All of these correlations can be considered weak for practical purposes; it is unlikely that any statistical model could be fit that would be useful for predicting contrast-detection threshold or psychometric function slope from either of the surrogate retinal ganglion cell measures.

Although many previous studies have examined the relationship between structural imaging data and visual function in glaucoma, there are limited published data on this relationship in healthy eyes. Garway-Heath et al.[30] reported data from 34 participants aged 58 ± 11 years with normal visual fields, finding no association between temporal neuroretinal rim area and central visual function measured by either perimetry or pattern electroretinogram. Hood and Kardon[31] examined relationships between visual function measured by perimetry in the superior and inferior arcuate areas and corresponding regions of RNFL thickness measured by OCT in 60 participants aged older than 50 years. They found only a weak correlation in both regions (superior arcuate region Pearson's correlation $r = 0.29$, inferior region $r = 0.22$).[31] Redmond et al.[32] measured both luminance increment detection and grating resolution acuity at 10° eccentricity in superior and inferior visual field (superior, 36° and 144° meridians averaged; inferior, 216° and 324° meridians averaged), and compared both to RNFL thickness measured by OCT in corresponding regions. Their 26 healthy participants were aged 51 to 77 years. The analysis carried out by Redmond et al.[32] primarily compared regression line slopes between healthy and glaucoma groups, and correlation coefficients were reported only for both groups combined. In common with the Hood and Kardon study,[31] the regression line had a positive slope between both functional measures and RNFL thickness in the healthy group alone, but the strength of the association (R^2 or correlation coefficient not reported) can be seen to be weak in their Figures 2, 3, and 4. Despite differences in participant ages, stimuli, test procedures, and test locations, all of these previous studies provide support for our finding of a very weak, or nonexistent, relationship between contrast-detection thresholds and current structural imaging measures in healthy observers.

The lack of association between contrast-detection thresholds and RNFL thickness in young, healthy participants has implications for the early detection of glaucoma. Glaucoma is often detected when either visual field or RNFL measurements fall outside normative database limits, and the stage of disease

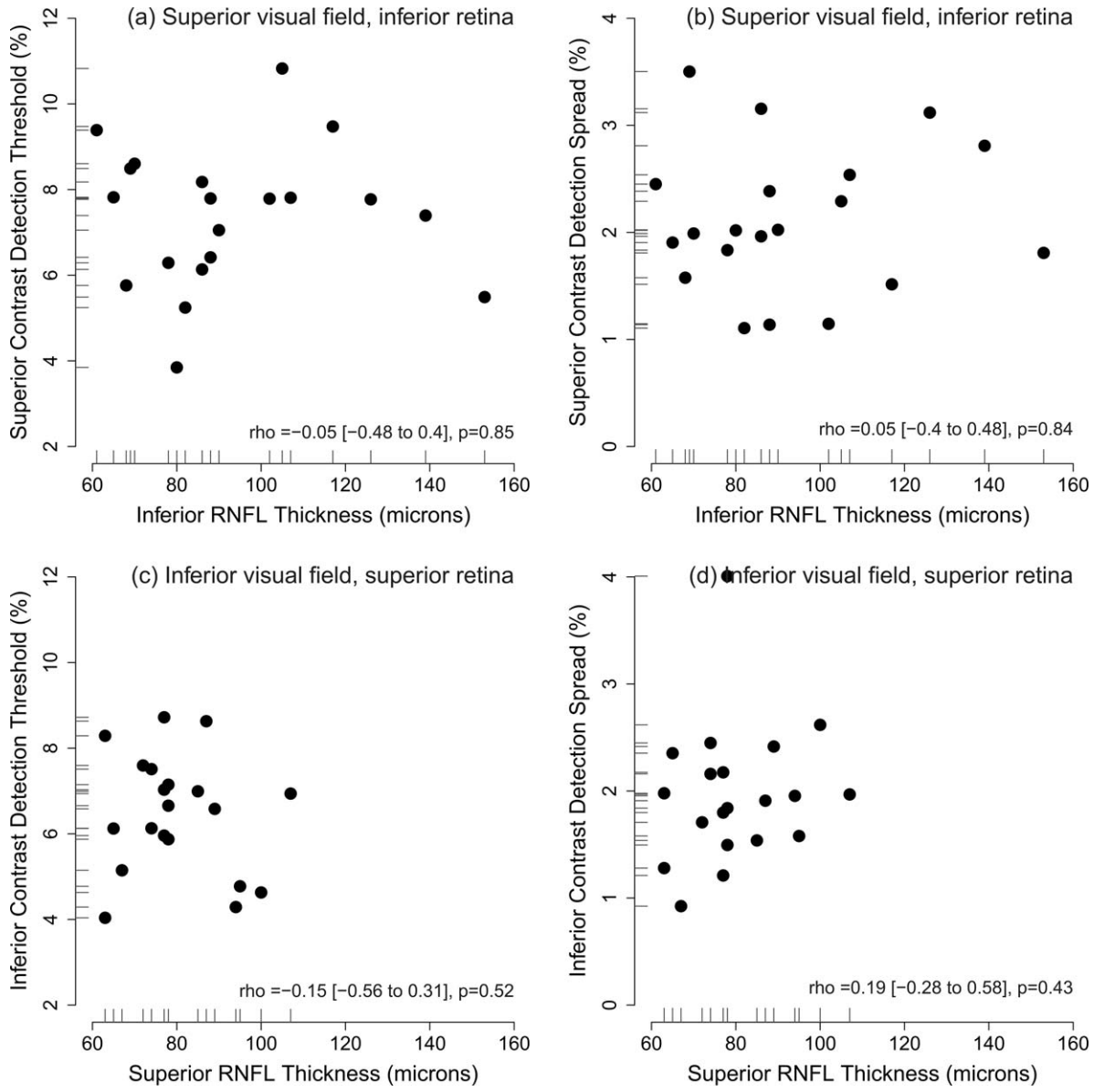

Figure 6. (**a**) Inferior RNFL thickness versus superior contrast-detection threshold, (**b**) inferior RNFL thickness versus superior contrast-detection psychometric function spread, (**c**) superior RNFL thickness versus inferior contrast-detection threshold, and (**d**) superior RNFL thickness versus inferior contrast-detection psychometric function spread. Spearman's correlations with 95% confidence intervals are given in each panel. *Gray lines* on the axes indicate distributions of the plotted values.

at which this happens for various imaging and functional measures has been the topic of considerable debate, as reviewed previously.[14,31,33] The present study shows that the baseline, predisease state of an individual patient could be high in the population distribution with one measure and low in the distribution with the other. With the simplifying assumption of equal progression due to glaucoma in both measures, the measure that started low in the population distribution would fall outside of the normal limits much earlier than the other measure. This implies that both structural and functional measures must be considered for early detection of glaucoma.

There are several reasons why the healthy population variation seen in RNFL thickness measured by OCT may not be an accurate reflection of the healthy population variation in the number of retinal ganglion cells. First, the RNFL contains a non-neural component (blood vessels, glia)[34–36] of variable thickness that remains present in eyes that are blind due to loss of retinal ganglion cells.[37–39] Further variability occurs in retinal ganglion cell axon diameters,[40,41] and the variation in axon density within the RNFL is currently unknown. These sources, in addition to simple measurement variability, will all contribute to the observed population variation in RNFL thickness and weaken any relationship between RNFL thickness and visual function. It is important to note, however, that there also are many more sources of variability in the visual system that could also account for the lack of a relationship with contrast-detection threshold and psychometric function spread. It is possible that any increase in signal due to greater numbers of retinal ganglion cells is countered by an equivalent increase in random noise. Pooling and processing of retinal ganglion cell signals in the lateral geniculate nucleus and visual cortex, as well as additional sources of internal noise in the visual system, are further unknowns in our study that are also

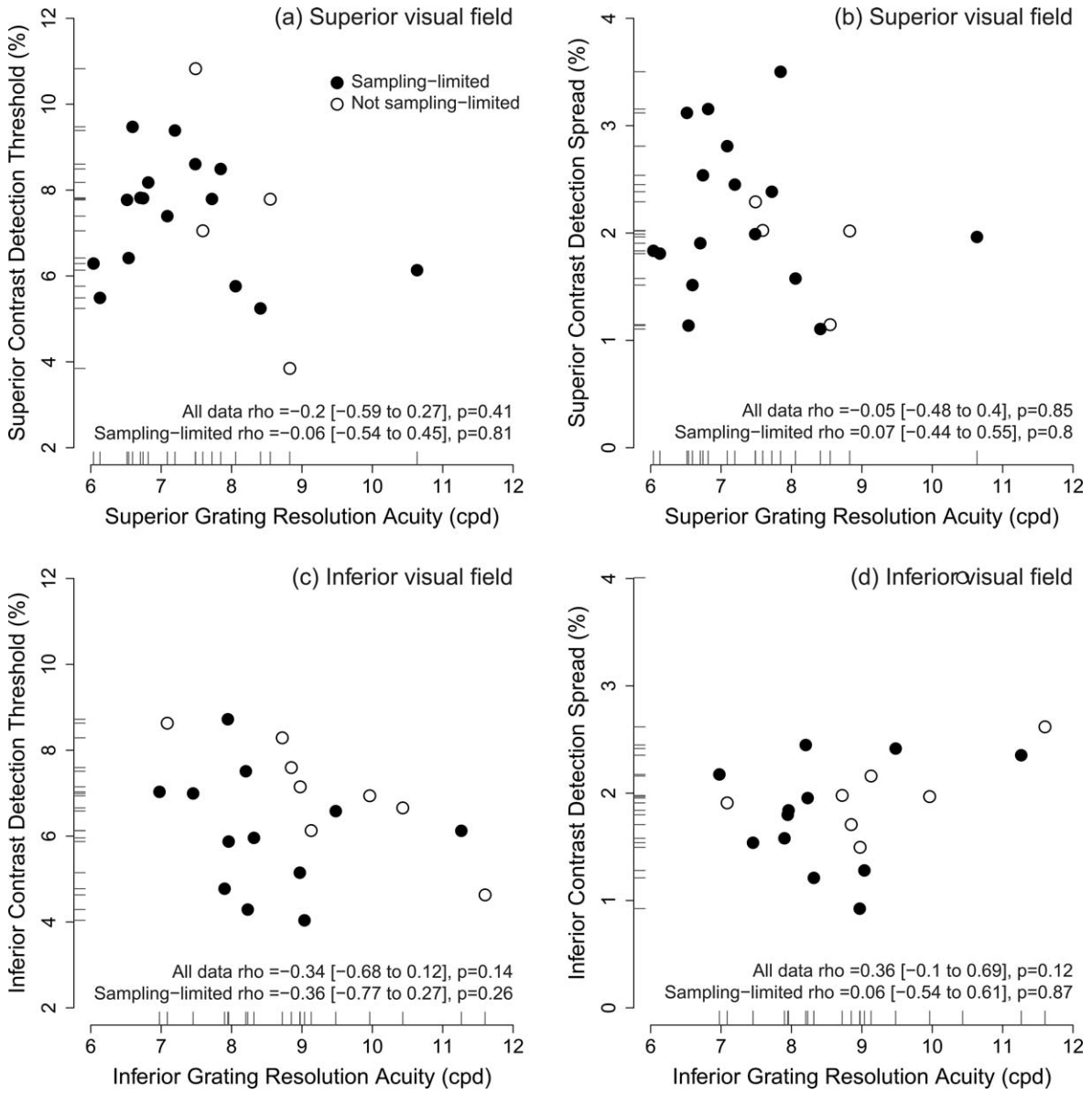

Figure 7. (**a**) Superior grating resolution acuity versus contrast-detection threshold, (**b**) superior grating resolution acuity versus contrast-detection psychometric function spread, (**c**) inferior grating resolution acuity versus contrast-detection threshold, and (**d**) inferior grating resolution acuity versus contrast-detection psychometric function spread. Locations that were sampling limited (as shown in Fig. 5) are shown as *filled circles*, nonsampling limited locations are shown as *unfilled circles. Gray lines* on the axes indicate distributions of the plotted values. Spearman's correlations with 95% confidence intervals are shown on each panel for all data, and also including only data from sampling-limited locations.

likely to vary among individuals, providing further sources of scatter in the relationships.

In this study, we chose to evaluate sectors of RNFL that were related to the visual field regions by a previously published model[27] that has been verified against manual tracing of retinal nerve fiber bundles with good concordance in the tested visual field regions.[42] The model customized these sectors to individuals, although across the range of anatomy in the sample the relevant sectors varied by only a small amount (Fig. 2). These sectors represent our current best estimate of the anatomical relationship between the tested visual field regions and the RNFL; however, it is worth noting that the sectors relate to larger, arcuate areas of the retina than are sampled by our Gaussian-windowed stimuli. It is possible to use the model to predict narrower regions of RNFL that relate somewhat more closely to the areas of the retina stimulated, but this method would be more vulnerable to small variations in the mapping,[29] and small eye movements during testing. It is not currently possible to isolate RNFL regions relating to visual field areas without also including RNFL regions along the arcuate path between the visual field area and the optic nerve head, and so we are making an assumption that the tested visual field locations are representative of the arcuate areas they sit within. Variation in the spatial distribution and axon size of retinal ganglion cells across the retina will therefore contribute scatter to the measured relationships. Fixation during the psychophysical testing was monitored visually; however, the accuracy of this is limited to approximately 2°, so we cannot rule out a contribution of small eye movements to the scatter found in the relationships reported. Although

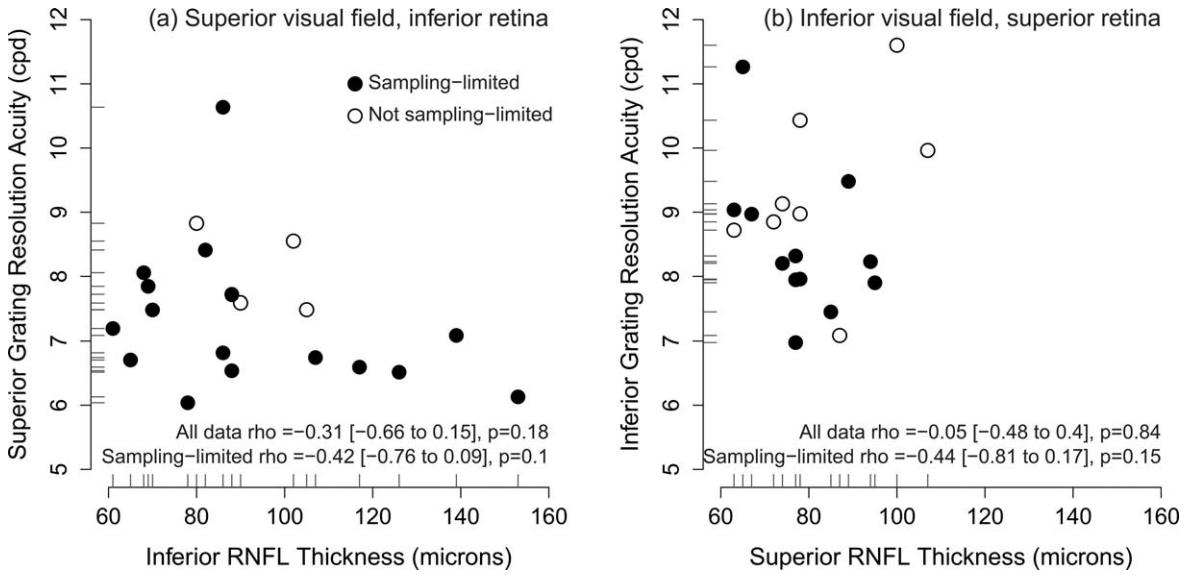

Figure 8. (**a**) Inferior RNFL thickness versus superior grating resolution acuity, (**b**) superior RNFL thickness versus inferior grating resolution acuity. Locations that were sampling limited (as shown in Fig. 5) are shown as *filled circles*, nonsampling limited locations are shown as *unfilled circles*. *Gray lines* on the axes indicate distributions of the plotted values. Spearman's correlations with 95% confidence intervals are shown on each panel for all data, and also including only data from sampling-limited locations

automated eye tracking would be an improvement to our methods, most of our observers had previous psychophysical experience, and fixation was not seen as problematic during testing.

As a final point, it is worth considering the sample size of 20 observers. In this study, we were specifically interested in whether a clinically meaningful relationship exists between the psychometric function for contrast detection and RNFL thickness. It is plausible that markedly increasing the sample size might render a statistically significant but weak correlation between these measures. However, given the variability in measurements among observers, such a relationship, if present, is unlikely to show any useful predictive power for an individual.

In conclusion, we have measured psychometric functions for contrast detection and compared these with surrogate measures of retinal ganglion cell number and density in a group of healthy young adults. Despite a 2- to 4-fold variation in all measures, we found no correlation between threshold or spread of the contrast-detection psychometric functions and either RNFL thickness or grating resolution acuity that could be exploited for predictive purposes.

Acknowledgments

Supported by Australian Research Council (ARC): ARC FT0990930 (AMM), ARC FT0991326 (AT), ARC LP100100250 (with Heidelberg Engineering), and ARC LP13100055 (with Heidelberg Engineering).

Disclosure: **J. Denniss**, Heidelberg Engineering (F); **A. Turpin**, Heidelberg Engineering (F); **A.M. McKendrick**, Heidelberg Engineering (F)

References

1. Enroth-Cugell C, Robson JG. The contrast sensitivity of retinal ganglion cells of the cat. *J Physiol*. 1966;187:517–552.
2. Shapley RM, Victor JD. The effect of contrast on the transfer properties of cat retinal ganglion cells. *J Physiol*. 1978;285:275–298.
3. Baccus SA, Meister M. Fast and slow contrast adaptation in retinal circuitry. *Neuron*. 2002;36:909–919.
4. Solomon SG, Peirce JW, Dhruv NT, Lennie P. Profound contrast adaptation early in the visual pathway. *Neuron*. 2004;42:155–162.
5. McKendrick AM, Badcock DR, Morgan WH. Psychophysical measurement of neural adaptation abnormalities in magnocellular and parvocellular pathways in glaucoma. *Invest Ophthalmol Vis Sci*. 2004;45:1846–1853.
6. McKendrick AM, Sampson GP, Walland MJ, Badcock DR. Contrast sensitivity changes due to glaucoma and normal aging: low-spatial-frequency losses in both magnocellular and parvocellular pathways. *Invest Ophthalmol Vis Sci*. 2007;48:2115–2122.
7. McKendrick AM, Sampson GP, Walland MJ, Badcock DR. Impairments of contrast discrimination and contrast adaptation in glaucoma. *Invest Ophthalmol Vis Sci*. 2010;51:920–927.
8. Sun H, Swanson WH, Arvidson B, Dul MW. Assessment of contrast gain signature in inferred magnocellular and parvocellular pathways in patients with glaucoma. *Vision Res*. 2008;48:2633–2641.
9. Lek JJ, Vingrys AJ, McKendrick AM. Rapid contrast adaptation in glaucoma and in aging. *Invest Ophthalmol Vis Sci*. 2014;55:3171–3178.
10. Chu PHW, Chan HHL, Brown B. Luminance-modulated adaptation of global flash mfERG: fellow eye losses in asymmetric glaucoma. *Invest Ophthalmol Vis Sci*. 2007;48:2626–2633.
11. Chauhan BC, Tompkins JD, LeBlanc RP, McCormick TA. Characteristics of frequency-of-seeing curves in normal subjects, patients with suspected glaucoma, and patients with glaucoma. *Invest Ophthalmol Vis Sci*. 1993;34:3534–3540.
12. Henson DB, Chaudry S, Artes PH, Faragher EB, Ansons A. Response variability in the visual field: comparison of optic neuritis, glaucoma, ocular hypertension, and normal eyes. *Invest Ophthalmol Vis Sci*. 2000;41:417–421.
13. Harwerth RS, Wheat JL, Fredette MJ, Anderson DR. Linking structure and function in glaucoma. *Prog Retin Eye Res*. 2010;29:249–271.

14. Malik R, Swanson WH, Garway-Heath DF. 'Structure-function relationship' in glaucoma: past thinking and current concepts. *Clin Experiment Ophthalmol*. 2012;40:369–380.
15. Denniss J, McKendrick AM, Turpin A. Towards patient-tailored perimetry: automated perimetry can be improved by seeding procedures with patient-specific structural information. *Trans Vis Sci Tech*. 2013;2:3.
16. Turpin A, McKendrick AM. Observer-based rather than population-based confidence limits for determining probability of change in visual fields. *Vision Res*. 2005;45:3277–3289.
17. Turpin A, Jankovic D, McKendrick AM. Identifying steep psychometric function slope quickly in clinical applications. *Vision Res*. 2010;50:2476–2485.
18. Curcio CA, Allen KA. Topography of ganglion cells in human retina. *J Comp Neurol*. 1990;300:5–25.
19. Daitch JM, Green DG. Contrast sensitivity of the human peripheral retina. *Vision Res*. 1969;9:947–952.
20. R Development Core Team. *R: A language and environment for statistical computing*. Vienna, Austria: R Foundation for Statistical Computing: 2012. Available at: http://www.R-project.org/. Accessed July 10, 2013.
21. Knoblauch K, Maloney LT. *Modeling Psychophysical Data in R*. New York, NY: Springer; 2012.
22. Wichmann FA, Hill NJ. The psychometric function: I. Fitting, sampling, and goodness of fit. *Percept Psychophys*. 2001;63:1293–1313.
23. Thibos LN, Cheney FE, Walsh DJ. Retinal limits to the detection and resolution of gratings. *J Opt Soc Am A*. 1987;4:1524–1529.
24. Thibos LN. Acuity perimetry and the sampling theory of visual resolution. *Optom Vis Sci*. 1998;75:399–406.
25. Anderson RS. The psychophysics of glaucoma: improving the structure/function relationship. *Prog Retin Eye Res*. 2006;25:79–97.
26. Turpin A, Sampson GP, McKendrick AM. Combining ganglion cell topology and data of patients with glaucoma to determine a structure-function map. *Invest Ophthalmol Vis Sci*. 2009;50:3249–3256.
27. Denniss J, McKendrick AM, Turpin A. An anatomically customizable computational model relating the visual field to the optic nerve head in individual eyes. *Invest Ophthalmol Vis Sci*. 2012;53:6981–6990.
28. Chauhan BC, Sharpe GP, Hutchison DM. Imaging of the temporal raphe with optical coherence tomography. *Ophthalmology*. 2014;121:2287–2288.
29. Denniss J, Turpin A, McKendrick AM. Individualized structure-function mapping for glaucoma: practical constraints on map resolution for clinical and research applications. *Invest Ophthalmol Vis Sci*. 2014;55:1985–1993.
30. Garway-Heath DF, Holder GE, Fitzke FW, Hitchings RA. Relationship between electrophysiological, psychophysical, and anatomical measurements in glaucoma. *Invest Ophthalmol Vis Sci*. 2002;43:2213–2220.
31. Hood DC, Kardon RH. A framework for comparing structural and functional measures of glaucomatous damage. *Prog Retin Eye Res*. 2007;26:688–710.
32. Redmond T, Anderson RS, Russell RA, Garway-Heath DF. Relating retinal nerve fibre layer thickness and functional estimates of ganglion cell sampling density in healthy eyes and in early glaucoma. *Invest Ophthalmol Vis Sci*. 2013;54:2153–2162.
33. Denniss J, Henson DB. The structure-function relationship in glaucoma: implications for disease detection. *Optom Pract*. 2009;10:95–104.
34. Ogden TE. Nerve fiber layer of the primate retina: thickness and glial content. *Vision Res*. 1983;23:581–587.
35. Hood DC, Fortune B, Arthur SN, et al. Blood vessel contributions to retinal nerve fiber layer thickness profiles measured with optical coherence tomography. *J Glaucoma*. 2008;17:519–528.
36. Patel NB, Luo X, Wheat JL, Harwerth RS. Retinal nerve fiber layer assessment: area versus thickness measurements from elliptical scans centered on the optic nerve. *Invest Ophthalmol Vis Sci*. 2011;52:2477–2489.
37. Sihota R, Sony P, Gupta V, Dada T, Singh R. Diagnostic capability of optical coherence tomography in evaluating the degree of glaucomatous retinal nerve fiber damage. *Invest Ophthalmol Vis Sci*. 2006;47:2006–2010.
38. Hood DC, Anderson S, Rouleau J, et al. Retinal nerve fiber structure versus visual field function in patients with ischemic optic neuropathy: a test of a linear model. *Ophthalmology*. 2008;115:904–910.
39. Hood DC, Anderson SC, Wall M, Raza AS, Kardon RH. A test of a linear model of glaucomatous structure-function loss reveals sources of variability in retinal nerve fiber and visual field measurements. *Invest Ophthalmol Vis Sci*. 2009;50:4254–4266.
40. Mikelberg FS, Drance SM, Schulzer M, Yidegiligne HM, Weis MM. The normal human optic nerve: axon count and axon diameter distribution. *Ophthalmology*. 1989;96:1325–1328.
41. Ogden TE. Nerve fiber layer of the primate retina: morphometric analysis. *Invest Ophthalmol Vis Sci*. 1984;25:19–29.
42. Denniss J, Turpin A, Tanabe F, Matsumoto C, McKendrick AM. Structure-function mapping: variability and conviction in tracing retinal nerve fiber bundles and comparison to a computational model. *Invest Ophthalmol Vis Sci*. 2014;55:728–736.

Investigative Ophthalmology & Visual Science